

# Surgical Treatment of Long-Bone Deformities: 3D Preoperative Planning and Patient-Specific Instrumentation

Philipp Fürnstahl, Andreas Schweizer, Matthias Graf,  
Lazaros Vlachopoulos, Sandro Fucentese, Stephan Wirth,  
Ladislav Nagy, Gabor Szekely and Orcun Goksel

**Abstract** Congenital or posttraumatic bone deformity may lead to reduced range of motion, joint instability, pain, and osteoarthritis. The conventional joint-preserving therapy for such deformities is corrective *osteotomy*—the anatomical reduction or realignment of bones with fixation. In this procedure, the bone is cut and its fragments are correctly realigned and stabilized with an implant to secure their position during bone healing. Corrective osteotomy is an elective procedure scheduled in advance, providing sufficient time for careful diagnosis and operation planning. Accordingly, computer-based methods have become very popular for its preoperative planning. These methods can improve precision not only by enabling the surgeon to quantify deformities and to simulate the intervention preoperatively in three dimensions, but also by generating a surgical plan of the required correction. However, generation of complex surgical plans is still a major challenge, requiring sophisticated techniques and profound clinical expertise. In addition to preoperative planning, computer-based approaches can also be used to support surgeons during the course of interventions. In particular, since recent advances in additive manufacturing technology have enabled cost-effective production of patient- and intervention-specific osteotomy instruments, customized interventions can thus be planned for and performed using such instruments. In this chapter, state of the art and future perspectives of computer-assisted deformity-correction surgery of the upper and lower extremities are presented. We elaborate on the benefits and pitfalls of different approaches based on our own experience in treating over 150 patients with three-dimensional preoperative planning and patient-specific instrumentation.

---

P. Fürnstahl · A. Schweizer · M. Graf · L. Vlachopoulos  
Computer Assisted Research and Development Group, University Hospital Balgrist,  
University of Zurich, Zurich, Switzerland

A. Schweizer · S. Fucentese · S. Wirth · L. Nagy  
Department of Orthopedic Surgery, University Hospital Balgrist, University of Zurich,  
Zurich, Switzerland

G. Szekely · O. Goksel (✉)  
Computer Vision Laboratory, ETH Zurich, Zurich, Switzerland  
e-mail: ogoksel@ethz.ch

## 1 Background

Bone and joint disorders are a leading cause of physical disability worldwide and account for 50 % of all chronic diseases in people over 50 years of age [1]. Among these, the degeneration of cartilage (i.e., osteoarthritis) is the most common disease [2], affecting 10 % of men and 18 % of women aged above 60 years [3]. The population is ageing thanks to increased life expectancy; accordingly, osteoarthritis is anticipated to become the fourth leading cause of disability by 2020 [3]. One reason of early arthritis development is abnormal joint loading induced by bone deformity [4, 5]; i.e., the shape of the bone is anatomically malformed. Reasons for bone deformity may be congenital, caused by a birth defect, or posttraumatic if the bone fragments heal in an anatomically incorrect configuration after a fracture (i.e., malunion). Besides the development of osteoarthritis, bone deformity may result in severe pain, loss of function, and aesthetic problems [6]. Particularly, gross deformities can cause quasi-impingement of the bones or increased tension in ligaments, resulting in a limited range of the motion. An unrestricted function is of fundamental importance for performing daily activities such as eating, drinking, personal hygiene, and job-related tasks. If not treated appropriately, salvage procedures such as *arthroplasty* (i.e., restoring the integrity and function of a joint such as by resurfacing the bones or a prosthesis) may be required.

Surgical treatment by corrective osteotomy has become the benchmark procedure for correcting severe deformities of long bones [6–9]. Particularly in young adults, a corrective osteotomy is indicated to avoid salvage procedures such as arthroplasty or fusion [10, 11]. In a corrective osteotomy, the pathological bone is cut and the resulting bone parts are correctly realigned (i.e., anatomical reduction), followed by stable fixation with an osteosynthesis implant to secure their position during bone healing. Treatment goal is the anatomy reconstruction—restoration of length, angular and rotational alignment, and displacement. However, osteotomy is technically challenging to manage operatively and hence it demands careful pre-operative planning. It is necessary to assess the deformity as accurate as possible to achieve adequate restoration. Conventionally, the deformity is quantified based on comparison, either to the healthy contralateral side [6, 12] if available or to anatomical standard values otherwise [13].

Three types of deformities are frequently encountered in an isolated or combined form and different types of osteotomies are performed to correct them [13, 14]: *Angular deformity* causes non-anatomical angulation of the distal and proximal bone parts. In general, angulation can occur in any oblique plane between the sagittal and the anterior-posterior planes. Isolated angular deformities are surgically corrected by performing a wedge osteotomy. In a closing wedge osteotomy, the bone is separated with two cuts forming a wedge which, when removed and closed, will correct the deformity. In contrast, in an opening wedge osteotomy one cut is made and the bone parts are aligned, resulting in a wedge-shaped opening. If the resulting gap is too large, which may result in implant failure due to instability, it is filled with structural bone graft to support healing before the parts are fixated [15].

A *rotational deformity* is characterized by an excessive rotation or twist of the bone around its longitudinal axis. That is, the distal segment shows a non-anatomic rotation around its own axis while the proximal part is considered as fixed. Rotational deformities can be corrected by performing a derotation of the fragment, often within a single osteotomy plane. If a *translational deformity* is present, the pathological bone is longer or shorter than it anatomically should have been. Accordingly, a lengthening or shortening osteotomy must be performed.

In practice, most deformities are a combination of the three types of isolated deformities, which makes preoperative planning and the surgery very challenging. A special type of long bone deformities are *intraarticular malunions* [16, 17], i.e., non-anatomical healing of the bone after joint fracture, resulting in gaps or steps on the articular surface. Intra-articular malunions can cause severe damage to the cartilage, making surgical treatment often necessary although the intervention is risky.

Conventionally, deformity assessment relies on plain radiographs or single computed tomography (CT) slices. Angular deformities and length differences are manually measured on plain X-rays in antero-posterior and lateral projections [6, 7]. In CT or magnetic resonance imaging (MRI), rotational deformities are assessed using proximal and distal cross-sectional images to compare torsion between the sides. The problem of the conventional technique is the assumption that a multi-planar deformity can be corrected by subsequently correcting the deformities measured in the anterior-posterior, sagittal, and axial planes separately, which is indeed an invalid assumption [18]. Accordingly, Nagy et al. [6] proposed to calculate the true angle of deformity in 3D space from planar measurements. Although feasible for angular deformities, their approach does not consider the rotational and translational components of a deformity.

Due to the above limitations of traditional approaches, computer assisted planning in 3D has become popular in orthopedic surgery as it permits to quantify a deformity by all 6 degrees of freedom (DoF)—3 translations and 3 rotations. Additionally, in contrast to emergency orthopedic treatments, corrective osteotomies are elective procedures scheduled in advance, therefore providing ample time for computer assisted planning. Since the first 3D osteotomy planning systems for the upper [19, 20] and lower extremities [21] had been described in the 90s, numerous approaches have been proposed for the 3D preoperative planning of long-bone deformities, i.e., osteotomies of the forearm bones, humerus, femur, and tibia. In these approaches, the basis for preoperative planning is a 3D triangular surface model of the patient anatomy generated from X-ray, CT, or MRI data of the patient. Based on the extracted 3D model, a preoperative plan can then be created by quantifying the deformity in 3D, followed by simulating the realignment to the normal anatomy. Dependent on the pathology and anatomy either the healthy contralateral limb, a similar-sized bone template, or anatomical standard values (e.g., axes, distances, and angles) can be used to determine normal anatomy. From a technical point of view, the alignment process to the normal anatomy using registration algorithms received most attention because the optimization target is easy to quantify. Apart from the fact that automatic alignment often achieves poor results, other aspects, such as the position of the osteotomy, are more difficult to

define in a standardized way as they do mainly rely on clinical parameters and the experience of the planner. However, all pre- and intra-operative aspects have to be jointly considered for developing a clinically feasible plan. Moreover, each deformity is unique and for this reason the surgical strategy differs from patient to patient, which complicates the development of standardized approaches.

Performing the surgery according to a complex preoperative plan can also be challenging. Missing anatomical reference points due to limited access to and view of the bone makes it almost impossible to perform a 6-DoF reduction without any supporting equipment. Therefore, navigation systems were proposed to execute the preoperative plan intra-operatively. Navigation systems have been used among different disciplines of orthopedic surgeries [22], particularly for bone realignment of the upper [23] and lower extremities [21, 24]. Although they offer superior accuracy [25], navigation systems have been losing popularity since they are costly and laborious to use. Originating from dental surgery [26] and thanks to recent advances in additive manufacturing, the production of patient-specific instruments has instead become a cost-effective and promising alternative to navigation systems [27]. Although the use of patient-specific guides for corrective osteotomies of long bones was described [11, 18, 28–34], the main application of patient-specific guides in orthopedic surgery is currently *arthroplasty* [35]. The key idea behind patient-specific guides is to design targeting devices specific to the anatomy and pathology of the patient for guiding the surgeon intra-operatively. Such patient-specific instruments are extremely versatile and, hence, particularly suited for the treatment of bone deformities because the surgical treatment varies between patients.

Within the last few years, we have successfully treated more than 150 patients by corrective osteotomy using a computer assisted approach. In this chapter, we report on the techniques developed and the experience gained in this field. First, in Sect. 2, the 3D preoperative planning process is described step-by-step, providing a guideline for performing this task in a standardized way. In Sect. 3, current patient-specific instruments required for performing different types of osteotomies are summarized. In Sect. 4, the treatment of intra-articular osteotomies using 3D planning and patient-specific instruments is demonstrated by means of a complex case. Lastly, our results on the accuracy and effort are given in Sect. 5 including a discussion of advantages and limitations of the presented techniques.

## 2 Pre-operative Planning and Surgical Technique

The most fundamental step of the computer-based planning is the quantification of the deformity in 3D. Dependent on the anatomy and pathology, we either use a template-based approach or an axis-based approach to determine the deformity and, subsequently, the required correction.

## 2.1 Template-Based Approach

Template-based approaches can be performed if the opposite limb is uninjured. In contrast to the lower limb, bilateral deformities are rarely observed for the upper extremities, making this approach particularly suited for the planning of deformities of the forearm (i.e., radius and ulna) and shoulder bones. As in the conventional method, computer assisted planning relies on the contralateral bone, which serves as a reconstruction template. The input data for the planning tool are 3D models generated from CT scans of the posttraumatic bone as well as the contralateral (healthy) bone. The segmentation is performed in a semi-automatic fashion using thresholding and region-growing algorithms of commercial segmentation software (Mimics, Materialise, Loewen, Belgium). Triangular surface meshes are generated from segmented CT scans using the Marching Cube algorithm [36]. Thereafter, the models are imported in our in-house developed planning-software CASPA (Balgrist CARD AG, Zurich, Switzerland).

In a first step of the planning, the model of the contralateral bone (i.e., the goal model) is mirrored using the sagittal plane as the plane of symmetry (Fig. 1a). Thereafter, a preliminary alignment to the goal model is performed to analyze the underlying deformity (Fig. 1b). Basic principles of comparing a pathological bone with a goal model in 3D are well known [18] and there are also clinically-established surface registration algorithms to facilitate this task. Briefly, the pathological bone is separated into (at least) two parts, both parts are aligned separately to the goal model, and their relative transformation  $T$  represents the amount of required reduction (Fig. 1b, c). In posttraumatic cases, a good starting point is to divide the bone into two regions proximal and distal to the former fracture line. Thereafter, point-plane iterative closest point (ICP) registration [37] is applied for aligning the proximal and

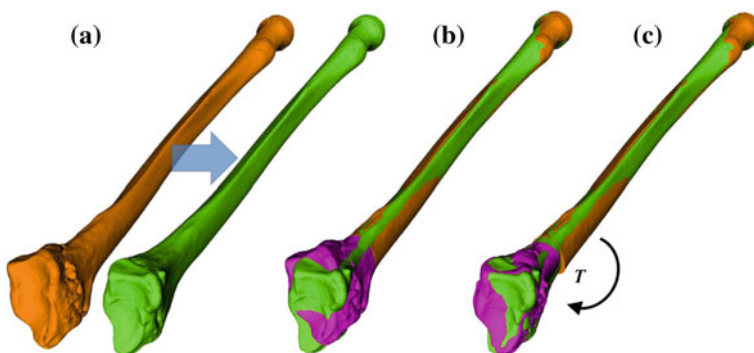


**Fig. 1** Template-based planning approach demonstrated for the radius bone. **a** Pathological radius (orange) and mirrored, contralateral bone (green) serving as the reconstruction template. **b** Aligning the proximal part (orange) to the goal model reveals the deformity (violet). **c** The reduction is simulated by subsequently aligning the distal part. The relative transformation  $T$  between the proximal and distal bone parts quantifies the amount of reduction (Color figure online)

distal bone parts with the goal model in an automatic fashion. In this ICP variant, the distance between each point of the source surface to the surface formed by the closest triangle on the target surface is iteratively minimized in a least squares sense. The required closest point queries can be efficiently performed with a KD-Tree [38]. In each ICP iteration, a distance threshold is computed for outlier identification, i.e., all closest point pairs which are above the threshold are discarded.

During this planning stage, potential side-to-side differences between the bones must also be identified and compensated because several studies showed that asymmetry between the left and the right limbs exist for long bones [39–41] such as in length and torsion. Asymmetry in size can be compensated easier for anatomy where the joint is formed by two bones (forearm: radius and ulna; lower leg: tibia and fibula). In such cases, the normal bones of both sides are compared to determine the size differences as demonstrated in Fig. 2. Thereafter, the goal model is first scaled by the same amount before its registration with the pathological bone.

A computer-planned corrective osteotomy does not involve only determining the optimal reduction, but also additional clinical factors crucial for a successful outcome shall be considered and optimized. After preliminary alignment, the surgeon is able to specify these parameters and constraints; e.g., possible access to the bone, osteotomy site, and type of the implant. Based on such specifications, the optimal surgical parameter values are determined in the planning tool: Besides the correction amount, the optimal selection of the osteotomy type, the position/orientation of the cutting plane(s), and the implant/screws position are important for a successful outcome and subsequent bone healing process.

A fundamental rule of conventional orthopedic planning is that a malunited bone is ideally cut at the apex of the deformity, which is the center of rotational angulation (CORA) [13] or the point of maximal deformity [7]. However, in practice a malunion has to be always regarded as a 3D deformity with 6 DoF to correct, hence restoring the normal anatomy requires one rotation—around a 3D axis often oblique to the anatomical standard planes—and one additional translation along a 3D displacement vector. While the direction  $r$  of the rotation axis can be calculated from

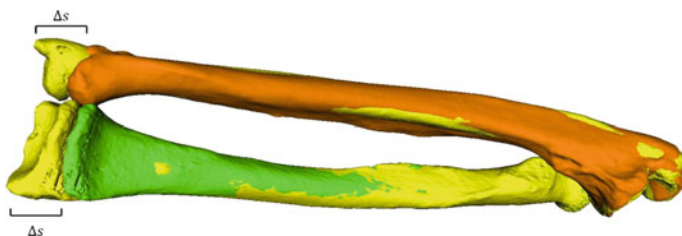


**Fig. 2** Compensation of length differences shown for the forearm bones radius and ulna. The normal ulna from the pathological side (pathological radius not shown) is denoted by *orange color*. The contralateral forearm bones are shown in *yellow*. The ulnae of both sides are compared to assess the length differences  $\Delta s$  between the *left* and *right* forearm. The contralateral radius is scaled by  $\Delta s$ , resulting in the goal model (*green bone*) used as the reconstruction template (Color figure online)

the rotation matrix  $R_{3 \times 3}$  of  $T$  [42], the center of rotation,  $C$ , can be chosen arbitrarily if no additional constraints are introduced. From the clinical point of view, it is desirable to choose the osteotomy site such that the fragments are minimally displaced after reduction to avoid creating gaps or steps at the osteotomy site. This can be achieved if  $C$  is close to the osteotomy site, on the one hand, and if  $C$  is only minimally translated after applying  $T$ , on the other hand. The latter holds true if  $\|T \cdot C - C\|$  is minimal. Decomposition of  $T$  yields the ill-posed minimization problem  $\min\|(I - R_{3 \times 3}) \cdot C - t\|$ , where  $t$  denotes the translational component of  $T$ . Further constraints can be introduced since any point on the desired axis would be a valid solution of the equation system  $(I - R) \cdot x = t$ . Additionally defining  $C$  as the point on the axis being closest to a reference point  $p_r$  (e.g., the center of the bone model) yields the equation with a unique solution

$$\begin{pmatrix} I - R \\ r \end{pmatrix} \cdot x = \begin{pmatrix} t \\ \langle p_r, r \rangle \end{pmatrix}$$

where the  $\langle \rangle$  operator denotes the inner product. The resulting axis  $(r, C)$  can be visualized in the planning application indicating the osteotomy position as demonstrated in Fig. 3.

The type of osteotomy and the orientation of the osteotomy plane directly influence how the bone surfaces will be in contact after reduction. Achieving maximum contact between the cortical bone layers of the fragments is strongly

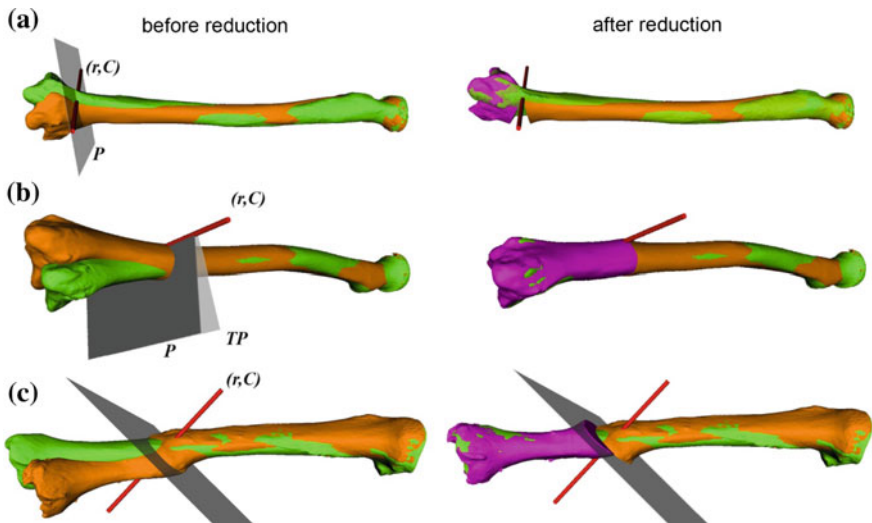


**Fig. 3** Different types of osteotomies planned in 3D. The rotation axis  $(r, C)$  and the osteotomy plane(s) are shown in red and grey, respectively. The pathological (orange) and contralateral bone (green) are given before (first column) and after (second column) simulated reduction. The reduced bone fragment is depicted in violet. **a** Distal radius opening wedge osteotomy. **b** Closing wedge osteotomy of the radius. **c** Single cut osteotomy of the tibia (Color figure online)

desired to promote healing. Again, the previously calculated axis ( $r$ ,  $C$ ) can provide a starting point to improve such contact.

As demonstrated in Fig. 3, a closing or opening wedge osteotomy is indicated if angular deformity is predominant; i.e., if the direction  $r$  is considerable different from the direction of the bone long axis. Adding or removing a bone wedge is also indicated if shortening or lengthening of the bone is required, i.e., a translation along the bone length axis between the aligned bone fragments was assessed. Given the osteotomy plane  $P$  and transformation  $T$ , the wedge is defined by  $P$  and  $T \cdot P$ , where the line of intersection between the planes represents the hinge of the wedge. As demonstrated in Fig. 3b, so-called incomplete closing wedge osteotomies can be preoperatively planned if  $P$  is oriented such that the line of intersection coincides with ( $r$ ,  $C$ ) Incomplete osteotomies are often preferred for bones of the lower limb, promoting bone consolidation and early loading. In this procedure, the bone is not entirely cut but a small cortical bone bridge remains, almost constraining the reduction to a rotation around the bone bridge (i.e., the hinge of the wedge). Vice-versa, the preoperatively planned reduction can be only achieved if the hinge corresponds to ( $r$ ,  $C$ ). More examples of this osteotomy type will be given later in Sect. 2.2. Dependent on the position of the hinge, a situation may arise where the wedge type is not clearly defined; i.e., part of the bones overlap while also a gap is created. For such situations, CASPA permits the visualization of the wedge in real time by simultaneously rendering  $P$  and  $T \cdot P$  on display. By doing so, the osteotomy plane can be interactively translated until the desired wedge osteotomy can be achieved.

If a rotational deformity is predominant, a so-called single cut osteotomy may be preferable to a wedge osteotomy. In this type of osteotomy, a single cut is performed which is pre-calculated such that sliding along and rotation in the cut plane permits reduction as planned [43]. An example of this osteotomy type is given in Fig. 3c. The position and orientation of a single cut osteotomy plane can be derived directly from the calculated reduction, i.e., the plane normal is defined by  $r$ . Although the single cut plane can be calculated exactly for any  $T$ , the osteotomy can be only applied if the translational component of  $T$  along the plane normal is negligible (i.e., below 1 mm) and the tangential translation is small, because otherwise either the bone contact surface would be too small or, worse, a gap between the bone parts would be created.

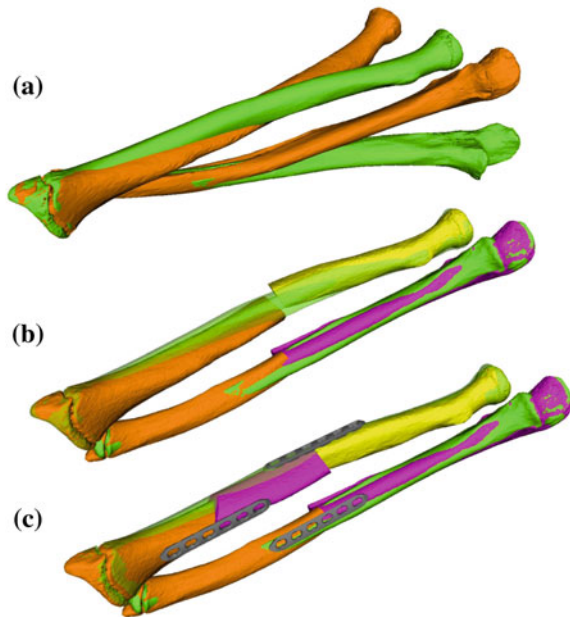
The inclusion of the osteosynthesis plate model, if available, into the preoperative plan, as demonstrated in Fig. 8a, can help to ensure a proper fitting of the plate. A poor plate fitting may result in less controlled procedure and decreased stability, which may lead to inaccurate reduction, delayed or stalled bone healing, or even implant failure. Inappropriately placed screws are another cause of delayed consolidation, and they may also harm the surrounding soft tissue. The best-fitting implant type can indeed be easily determined in the planning tool and also the optimal position of such implant can already be defined preoperatively. Optimally, the implant also contains the position and direction of the screws. The screw models



are used by the surgeon to verify that all screws will be placed sufficiently inside the bone but without penetrating the osteotomy plane or anatomical regions at risk.

In severe deformities, one osteotomy may not be sufficient to achieve a satisfactory result. In such cases, multiple mutually-dependent osteotomies must be performed, resulting in a considerable increase in the complexity of the preoperative plan. As demonstrated in the example case given in Fig. 4, we propose a step-wise approach in such cases. The 14-years-old patient suffered from a post-traumatic malunion of both forearm bones, resulting from a fall four years ago. The deformity was assessed by aligning the distal third of each pathological bone to the contralateral model using ICP (Fig. 4a). Next, mid-shaft osteotomies at the apex of the deformity were performed for both radius and ulna, and the reduction was simulated by registering the proximal parts to the goal models using ICP. As shown in Fig. 4b, the resulting reduction of the radius fragment was not acceptable from a clinical point of view, due to the large gap and cortical surface mismatch on the radius. Therefore, an additional osteotomy was defined in the distal third of the radius and the resulting fragment was manually aligned to the goal model. In a second iteration, the transformation between the bone fragments and the osteotomy sites were fine-tuned in a manual fashion in order to achieve correct alignment by applying only single-cut osteotomies. The final result, given in Fig. 4c, was obtained after recalculating the surgical plan.

**Fig. 4** Stepwise preoperative planning of a triple osteotomy for treating a complex deformity affecting both bones of the forearm. The reconstruction template is shown in *green*. **a** First step: radius and ulna were distally aligned to the template. **b** Second step: for both bones mid-shaft osteotomies were performed. **c** Third step: final result after an additional radius osteotomy (Color figure online)



## 2.2 Axis Realignment

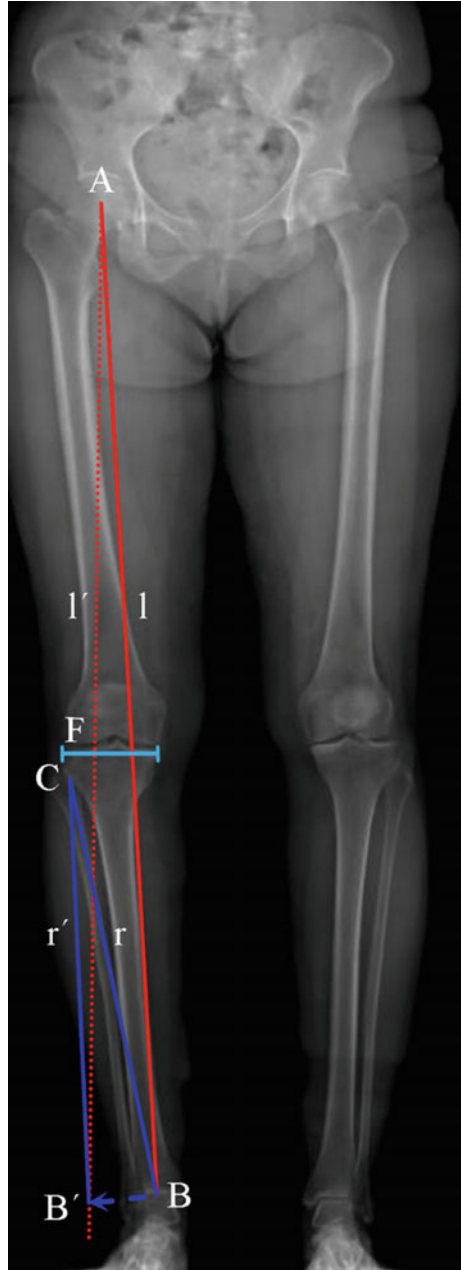
Realignment of the lower limb is primarily indicated in patients having a varus- (out-knee) or valgus-deformity (in-knee), resulting in a pathologically deviated weight-bearing line of the leg (i.e., the mechanical axis) [13]. In many cases, the deformity is caused by a congenital defect affecting both limbs and, therefore, the contralateral bone cannot be used as a reconstruction template. Instead, the required correction is determined by realigning the mechanical axis to its anatomically normal position. According to Paley et al. [13], the mechanical leg axis passes not exactly through the knee joint center, but is located  $8 \pm 7$  mm medial to the knee joint center. This deviation is called mechanical axis deviation (MAD) and is measured as the perpendicular distance from the mechanical leg axis to the knee joint center. A malalignment can be considered as pathological if the MAD lies outside of this normal range.

Before describing the 3D method for the preoperative planning of axis realignment procedures, the conventional approach is next briefly summarized. In the conventional preoperative assessment, long-leg standing X-rays are acquired for determining pathological and normal mechanical leg axes, as depicted in Fig. 5. Based on these axes, the position  $C$  and opening angle  $\varphi$  of a corrective osteotomy is calculated using a method described by Miniaci et al. [44]. In a first step, the preoperative mechanical leg axis  $l$  is determined as the straight line from the hip joint center  $A$  to the upper ankle joint center  $B$ . The postoperative axis  $l'$  can be calculated by considering the fact that it should pass through a point  $F$  on the tibia plateau, at 62 % of the plateau width measured from medial (for varus-deformity). Point  $F$  is the so-called Fujisawa point, named after the author of the study [45], in which the optimal intersection point between the mechanical leg axis and the tibial plateau was investigated. The position of the rotation center of the osteotomy  $C$  is dependent on the pathology (e.g., closing/opening tibial/femur osteotomy). After the center of the osteotomy  $C$  is defined by the surgeon, the angle  $\varphi$  can be calculated. For this purpose,  $C$  is connected by the line  $r$  with the preoperative upper ankle joint center  $B$ . Lastly, the postoperative ankle joint center  $B'$  and, correspondingly, the osteotomy angle  $\varphi$  are determined by rotating  $r$  around  $C$  until it intersects with the postoperative axis  $l'$  at point  $B'$ .

We have developed a method for quantifying the required 3D osteotomy parameters (i.e., position, rotation axis, and angle). Our approach requires having triangular surface models of the hip, knee, and ankle joints. We apply a CT protocol that scans the regions of interests while skipping the irrelevant mid-shaft regions to reduce radiation exposure. Based on the CT scan, a limb model consisting of the proximal femur, distal femur, patella, proximal tibia, distal tibia, distal fibula and talus, is reconstructed. Thereafter the hip, knee, and ankle joint centers of the limb model have to be determined in 3D before the mechanical axes can be calculated.

The joint center of the proximal femur  $A$  is defined by the center of the best fitting sphere [46], minimizing the distance to a user-selected region of the femoral head points, as demonstrated in Fig. 6a. The bone model of the proximal tibia is

**Fig. 5** Measurement of the pathological mechanical leg axis  $l$  and calculation of the realigned normal axis  $l'$  in 2D



used to determine the center of the knee joint and an analytical description of the tibia plateau plane  $P_{tib}$  (Fig. 6b), both required for computing the Fujisawa point. We follow Moreland [47] who defined the knee joint center as the midpoint

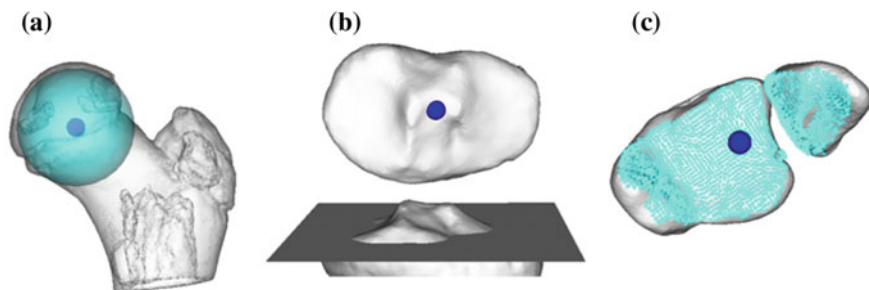
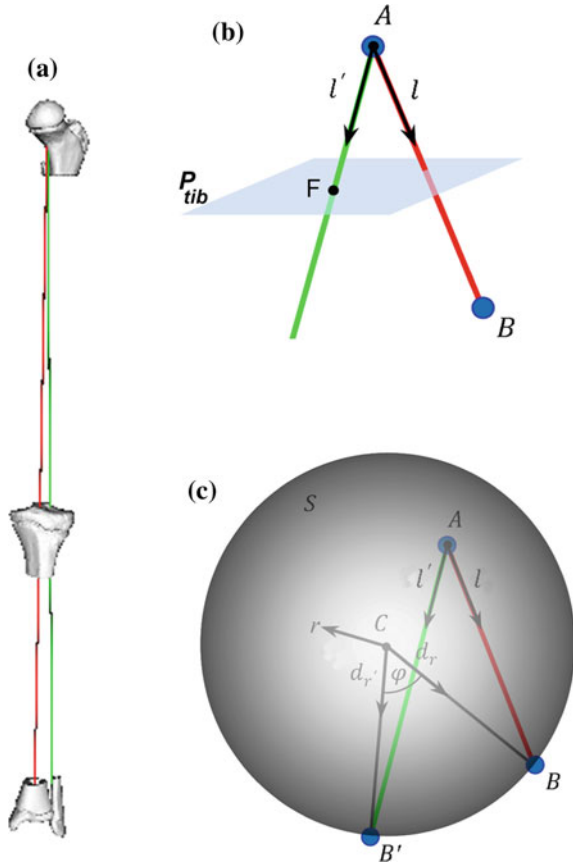


**Fig. 6** Determination of the relevant joint parameters. **a** The center of the femoral head is calculated by the center (dark blue) of the best fitting sphere (cyan). **b** Knee joint center (dark blue) and tibia plateau plane  $P_{tib}$  (dark grey). **c** The ankle joint center (dark blue) is defined as the center of mass of the articular surface (cyan points) (Color figure online)

between the intercondylar eminences of the tibial plateau. As for the femur, a least squares approach is applied for finding the plane  $P_{tib}$ , minimizing the distance to user-selected plateau regions as depicted in Fig. 6b. Lastly, the center of ankle joint  $B$  is calculated as demonstrated in Fig. 6c. The ankle center can be anatomically described as the midpoint between the medial and lateral malleolus [47], i.e., the center of the articular surface of both tibia and fibula with respect to the talus bone. Accordingly, we propose a method for calculating the 3D ankle joint center by analyzing the opposing articular surfaces between these bones. First, tibia and fibula points having a small distance to the talus bone are identified, because they are potential candidates for being articular surface points. These candidate points are efficiently found by calculating the closest-point distance to the talus bone model using a KD-tree [38] and considering only points below a user-defined distance threshold. A second criterion is introduced to eliminate false positive candidate points: All candidates, for which the angle between its surface normal vector and the direction vector to its closest point on the talus surface is above a user-defined threshold, are eliminated. Both thresholds are visually determined per case until the entire articular surface is detected as shown in Fig. 6c. Typically the distance and angle thresholds are between 4–8 mm and  $40^\circ$ – $70^\circ$ , respectively. The joint center is finally computed as the center of mass of all selected points on the tibia and fibula surface.

After the joint centers are calculated, the pathological and corrected mechanical axes  $l$  and  $l'$  can be calculated in 3D (Fig. 7a–c). As depicted in Fig. 7b, axis  $l$  is defined as a straight line from the hip joint center  $A$  to the ankle joint center  $B$ . Axis  $l'$  is defined by the direction vector from  $A$ , passing through the Fujisawa point  $F$  on  $P_{tib}$ . For performing the desired correction, the osteotomy axis  $r$  must be perpendicular to the plane of deformity spanned by  $l$  and  $l'$ ; i.e.,  $r = l \times l'$ . The postoperative ankle joint center  $B'$  and the osteotomy angle  $\varphi$  can be calculated by solving the line/sphere intersection problem shown in Fig. 7c. That is, since the length of the leg axis should not change,  $B'$  is located on the sphere  $S$  with the center  $C$  and radius  $|CB|$ , i.e. at the intersection of axis  $l'$  with  $S$ . Once  $B'$  is determined, the

**Fig. 7** Measurement of the pathological mechanical leg axis  $l$  and calculation of the realigned normal axis  $l'$  in 3D. **a** Mechanical leg axis before (red) and after (green) realignment. **b** Calculation of the Fujisawa point  $F$  for determining the direction of the postoperative leg axis  $l'$ . **c** Calculation of the postoperative ankle joint center  $B'$  (Color figure online)



osteotomy angle  $\varphi$  is computed from the angle between the direction vectors  $d_{r'}$  and  $d_r$  (Fig. 7c).

One benefit of the 3D approach is that the axis realignment does not only encode the deformity correction in the anterior-posterior plane, but it also indicates the correction in the sagittal plane, if desired (e.g., for the correction of the tibial slope). Once the quantitative planning parameters are defined, an opening or closing wedge osteotomy can be simulated as in the template based approach. Examples of an opening wedge proximal tibia osteotomy and a closing wedge distal femur osteotomy are given in Fig. 8. The transformation from  $B$  to  $B'$  can be expressed by a matrix  $T$ , representing the amount of the required reduction. The osteotomy plane  $P$  is then uniquely defined by the axis ( $r, C$ ) forming the hinge of the wedge (see Fig. 8b). The planning tool shall allow for interactive positioning and fine-tuning of the osteotomy plane, because the optimal position is dependent also on the soft-tissue anatomy and the particular pathology of the patient. Note that  $\varphi$  must be recalculated after moving the plane and the axis to a new axis position, because the opening angle is dependent on the position of the axis.

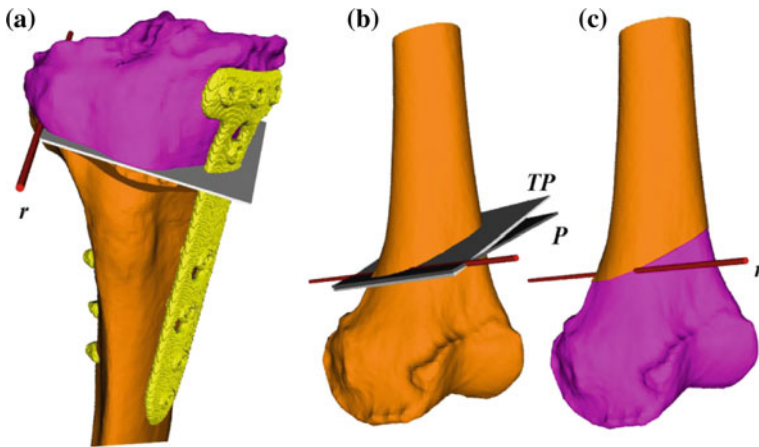


**Fig. 8** Osteotomies performed for realignment of the mechanical axis of the leg. **a** Opening wedge osteotomy of the proximal tibia. The exact position of the osteosynthesis plate (yellow) is preoperatively planned as well. **b** and **c** Closing wedge osteotomy of the distal femur before (**b**) and after reduction (**c**). The wedge is formed by the osteotomy plane *P* and *TP* (Color figure online)

### 3 Surgical Technique and Guides

Creation of a computer assisted surgical plan and the implementation of the plan using a specific surgical technique go hand in hand and cannot be considered separately. On one hand, the surgical technique and strategy must be known before developing a preoperative plan. On the other hand, it must be possible to realize a preoperative plan without risk and with state-of-the-art surgical techniques. For multi-planar deformities, the reduction task is often too complex to be performed conventionally without additional tools supporting the surgeon. We use patient-specific instruments in the surgery, enabling the surgeon to reduce the bone exactly as planned on the computer. These so-called *surgical guides* have proved successful over years in different orthopedic interventions. The basic principle is that the body of a guide is shaped such that it can be uniquely placed on its planned position on the bone by using characteristics of the irregular shaped bone surface and it helps intra-operatively to define the osteotomy plane and correction.

Each malunion and, consequently, each surgery is different which makes not only preoperative planning but also patient-specific instrumentation challenging. The goal is to develop guides that are sufficiently flexible to be applied to various types of osteotomies, but nevertheless enabling generation in a standardized and time-efficient way. In our experience, patient-specific guides have to be considered as an integral part of the surgical plan; i.e., they should be designed in the planning tool to define the osteotomy position, the direction of the cut, the position of the

implant, and the relative transformation of the fragment after reduction. The CASPA tool enables the generation of the guides in a semi-automatic fashion. In a first step, the guide body is created based on a 2D outline drawn around the osteotomy location on the bone surface. It is crucial that this step is performed by a surgeon, because the guide surface must not cover soft-tissue structures (e.g., ligaments) that cannot be removed from the bone for guide placement. To generate a 3D guide body, the outline is extruded normal to the bone surface by a user defined height, followed by boolean subtraction of the bone surface [48]. To achieve a unique fit, the shape of the guide body is designed to contain irregular convex and concave parts covering the bone from different directions.

As demonstrated in Fig. 9, we have developed different cutting guides to support the surgeon in performing osteotomy. One way of defining the cut position and direction is to use a metallic inlay (Fig. 9a) that contains a cutting slit to guide the saw blade. The inlay is inserted into a dedicated frame in the guide body for alignment according to the planned osteotomy plane. Although very accurate, the technique is limited to certain saw blade types and it requires the bone to be sufficiently exposed. Alternatively, a cutting slit can be directly integrated into the plastic guide or the edge of the guide body can be used for guiding the saw blade (Fig. 9b). These types of cutting guides are particularly helpful for performing closing wedge osteotomies, where the distance between the two cuts may be very small. Lastly, K-wires set by a drilling guide can be used to approximate the osteotomy plane. In this case, the direction of the saw blade can be also controlled inside of the bone.

In our experience, two different approaches have been proven to be successful for supporting correct realignment of the bone fragments with the help of patient-specific reduction guides. In one method, separate reduction guides are used

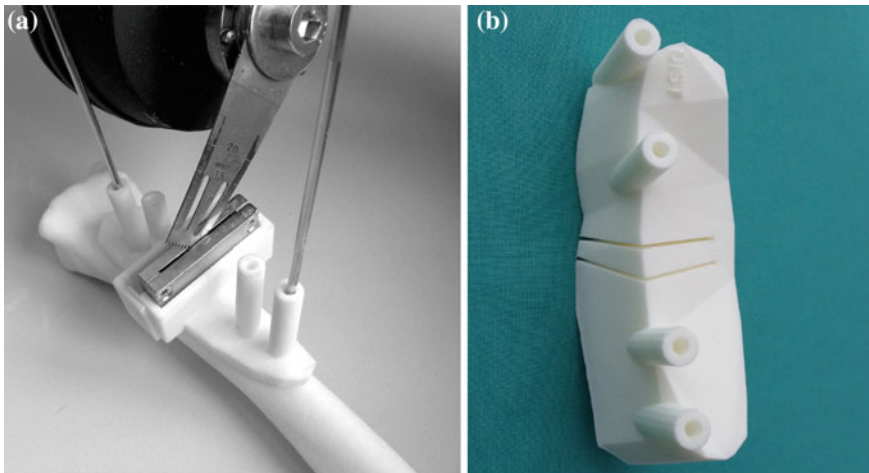


**Fig. 9** Different types of cutting guides for guiding the saw blade. **a** Metallic inlay with a cutting slit. **b** Cutting slit directly integrated in the plastic guide body

to predefine the reduction by their shape. To do so, two guides combined with K-wires are required in the surgery (see Fig. 10). First, a reduction guide is generated in CASPA based on four parallel K-wires that are positioned on the fragments in their reduced positions. This guide uniquely defines the relative transformation between the fragments after reduction. Next, the K-wires are transformed back to the pathological bone by applying the transformation  $T^{-1}$ , and, accordingly, a guide is constructed. In the surgery, the latter guide is applied first to set the K-wires before the osteotomy, as demonstrated in Fig. 10a. After the osteotomy (Fig. 10b), the reduction guide is inserted over the K-wires to move the fragments to their planned positions (Fig. 10c), followed by plate fixation (Fig. 10d).

Note that, if K-wires are considerably divergent, a multi-part guide is required to allow for the removal of the guide. For this reason, we have developed multi-part guides that can be stably connected but removed separately. As shown in Fig. 10a, the first variant results in a very stable connection between the parts due to cylinders that are plugged into corresponding holes in the opposite guide parts. The cylinders must point in the same direction as the K-wires to permit removal of the guide part after K-wire insertion. The system can be used only for guides which are sufficiently high (e.g., 1 cm). Alternatively, a V-shaped connector as shown in Fig. 10b can be applied if the space for the guide is limited (Fig. 11).

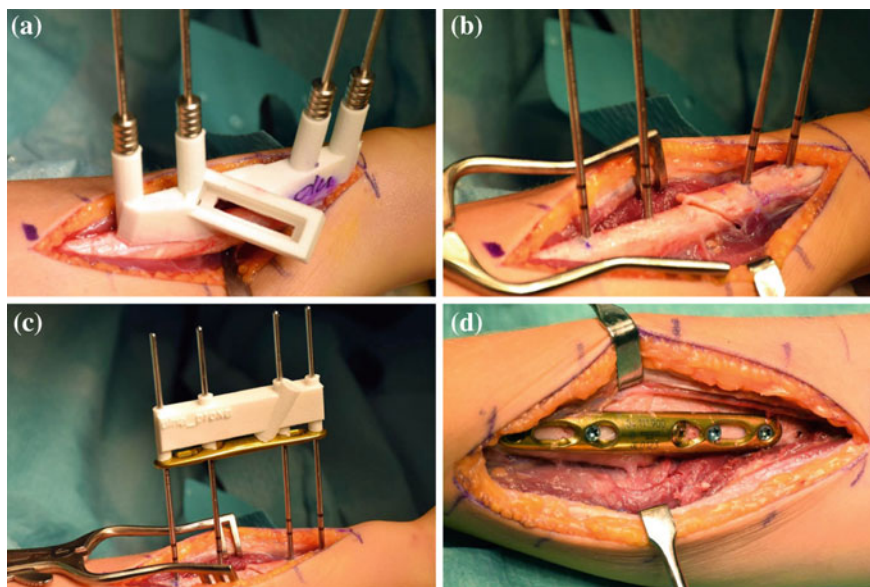


**Fig. 10** Reduction guides based on K-wires. **a** K-wires are set before the osteotomy using dedicated drill sleeves. **b** The osteotomy is performed. **c** After osteotomy, a guide is used to move the K-wires and, consequently, the mobilized fragments into their planned position. **d** Fixation with an implant



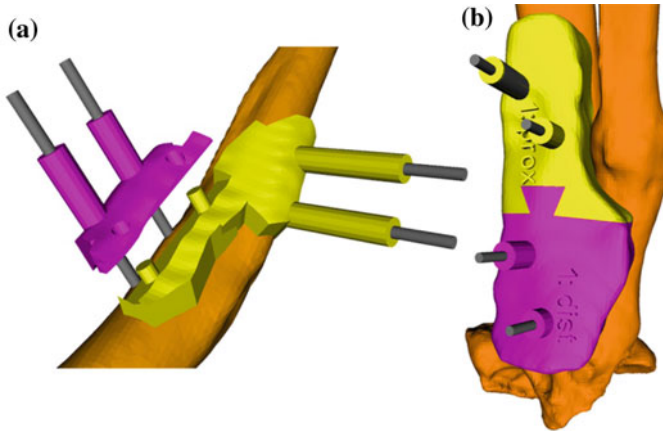


**Fig. 11** Multi-part guides where each part can be removed separately in case of divergent K-wires. **a** Variant using cylinders that are plugged into corresponding holes in the opposite part. **b** Variant using a V-shaped connecting surface

Another approach is to directly utilize the implant (i.e., the osteosynthesis plate) for supporting the surgeon in the reduction task. The most straight-forward way is to manufacture a 1:1 replica of the reduced bone to prebend the plate according to the bone shape (see Fig. 12). Plate prebending is a common method in conventional orthopedics to define the transformation of the fragments in their reduced position. Although effective, the method has limited accuracy because it does not fully constrain all DoF.

Athwal et al. [23] introduced a more sophisticated and accurate technique based on a navigation system to realign the fragments using the screws of the fixation plate. We [32] and others [28, 29] have further developed this technique by applying patient-specific guides to avoid the use of a navigation system. The method requires the use of an implant based on angular-stable locking screws. Locking screws have the property that threads on the screw head lock into corresponding threads of the screw holes in the plate, resulting in an angular and axial

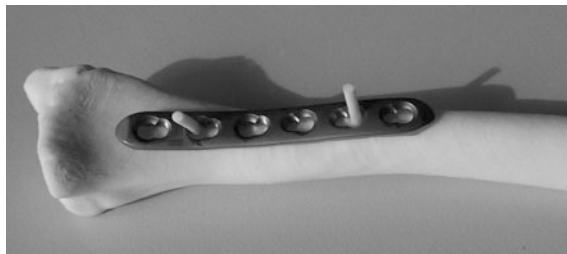


**Fig. 12** Osteosynthesis plates can be prebent before surgery based on a real-size bone model. The model is generated by additive manufacturing the reduced bone after simulated osteotomy

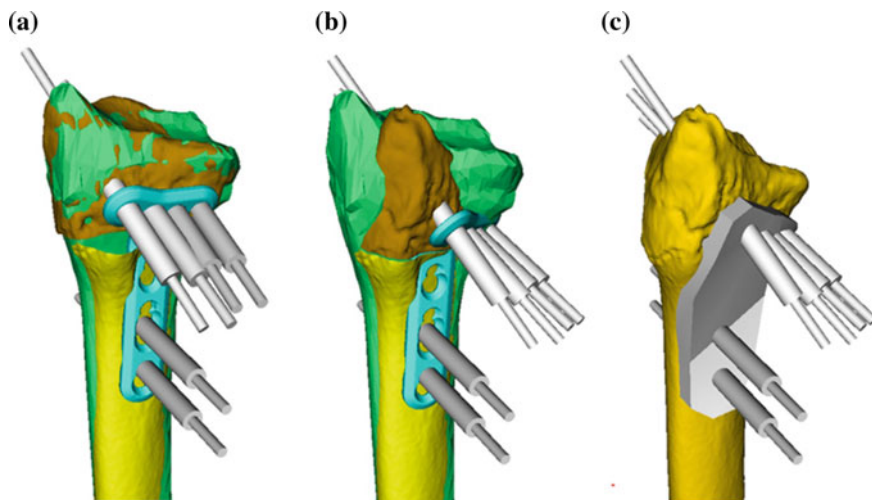


**Fig. 13** Reduction via the screws of the implant. The cut bone fragments of the pathological radius are shown in *brown* and *yellow*, respectively. The contralateral mirrored bone is shown in *green*. **a** Implant (*cyan*) is positioned on the bone fragments after simulated osteotomy. Grey cylinders represent the angular-stable locking screws. **b** The screws are transformed back to uncorrected bone by applying the inverse reduction. **c** A guide with drilling sleeves is created based on the screws (Color figure online)

stable screw anchorage. Therefore, the plate maintains distance to the bone during fixation, in contrast to compressing plates where the fragment is pulled towards the plate. For this purpose, a locking system is particularly suited for integration into a computer-based surgical planning as the bone-plate-screw interface is uniquely defined. The preoperative planning method is similar to the one using reduction guides based on K-wires. After the plate model is positioned on the bone surface in postoperative configuration (Fig. 13a), the screw models are transformed back to their preoperative position by applying transformation  $T^{-1}$  (Fig. 13b), and used for creating a drilling guide which has drill sleeves for the screws (Fig. 13c). In the surgery, the guide is applied before the osteotomy to drill the screw holes, as shown in Fig. 14a. After cutting the bone, the plate is first fixed to one fragment using the predrilled holes and, subsequently, the other fragment is reduced as planned by fixation to the plate (Fig. 14b).

Using additive manufacturing, patient-specific instruments can be produced based on 3D models designed in the planning application. In our case, the guides are manufactured by Medacta SA (Castel San Pietro, Switzerland) using a selective laser sintering device (EOS GmbH, Krailling, Germany). The guides are made of medical-grade polyamide 12. They are cleaned with a surgical washer and sterilized using conventional steam pressure sterilization at our institution.

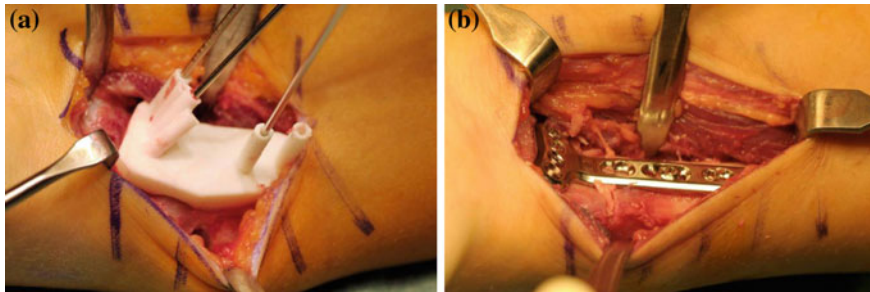


**Fig. 14** Patient-specific guide for pre-drilling the screw holes. **a** The screw holes are pre-drilled before the osteotomy. **b** After osteotomy, the fragments are reduced as planned by fixation to the plate

## 4 Intraarticular Osteotomies

Corrective osteotomies of intra-articular malunions are among the most challenging orthopedic procedures with respect to both preoperative planning and surgery. The limited access to the joint surface makes an inside-out-osteotomy (i.e., cutting from the joint surface towards the shaft) difficult or, in certain settings, even impossible. An extra-articular, outside-in approach to the intra-articular malunion provides an alternative in the surgical treatment. However, such a technique requires extensive preoperative planning and, moreover, the surgeon must be guided intraoperatively because he has no direct view into the joint. We have developed a preoperative planning methodology combined with a closely-linked surgical technique [11], enabling the surgeon to perform an outside-in approach in a controlled way. We will describe the approach based on one of the most complex cases treated at our institution so far.

The 62 year old patient sustained a distal radius fracture that had been insufficiently treated at another institution by open reduction and internal fixation with palmar plating. As demonstrated in (Fig. 15a), the CT-reconstructed 3D model of the pathological radius showed steps and gaps up to 4 mm in the joint surface area, well visible, especially if compared to the opposite mirrored normal bone. The 3D analysis based on the former fracture lines and the contralateral bone identified 3 intraarticular fragments and an overall shortening of the radius. The coarse pre-operative plan depicted in (Fig. 15b) intended to align the styloid fragment (denoted by the dark blue fragment) and the central palmar fragment (light blue fragment) to the lunate facet fragment (purple arrow), which was initially left fixated to the radius shaft. Before simulating the osteotomies, the exact cut planes had to be defined. To do so, consecutive line segments were specified by the surgeon along the former fracture lines of the joint surface. Thereafter, the corresponding 3D osteotomy planes were automatically generated by extrusion of the line segments. Next, the surgeon defined the extra-articular entry point of the cut planes respecting the best access through the soft tissue by rotating the osteotomy planes around the

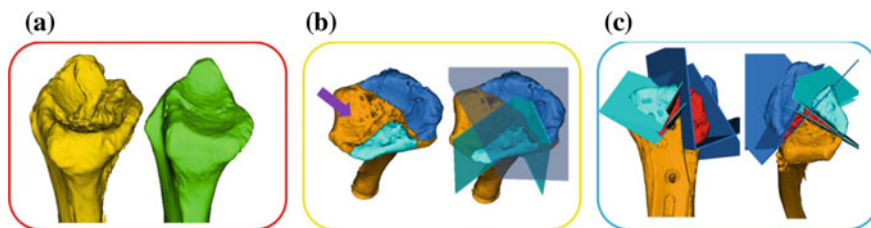


**Fig. 15** Definition of the cut planes for an intra-articular osteotomy. **a** Pathological radius (*yellow*) compared to the mirrored, contralateral bone (*green*). **b** Three cut planes are required for mobilization of the fragments. The purple arrow denotes the lunate facet fragment. **c** Additional cut planes are calculated, necessary to remove bone parts that would overlap after reduction (Color figure online)

previously defined line segments. The final cut planes planned for fragment mobilization are shown in Fig. 15b. Thereafter, the fragments were interactively and consecutively aligned to the normal bone in their correct anatomical position to restore a congruent joint surface (Fig. 16). Based on the fragment positions in their original and reduced positions, the planning software CASPA also enables the automatic calculation of the offcut (Fig. 16a), which should be removed (i.e., closing wedge osteotomy). In total six cutting planes, i.e., three planes for mobilizing the fragments and three for removing the offcut, were required in this case as shown in Fig. 15c.

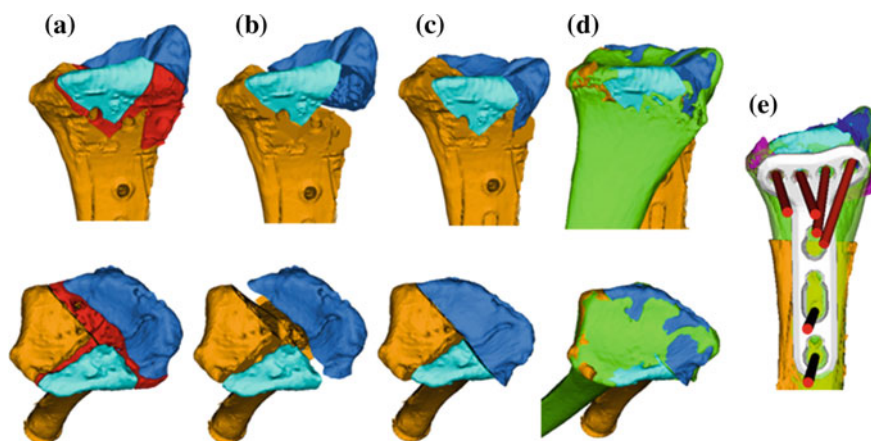


**Fig. 16** Reduction of a complex intra- (**a–d**) and extra-articular (**e**) malunion. *Top row* Palmar view. *Bottom row* axial view. **a, b** Fragments in their pathological positions before and after removal of the offcut (*red*). **c** Fragments in their reduced positions. **d** Overlay with the mirrored contralateral bone (*green*), demonstrating joint congruency but a residual shaft deformity. **e** Result after intra- and extra-articular osteotomy compared to the contralateral bone (*green, transparent*). The *red cylinders* denote the directions of the angular stable locking screws of the osteosynthesis plate used for fixation (*grey*) (Color figure online)

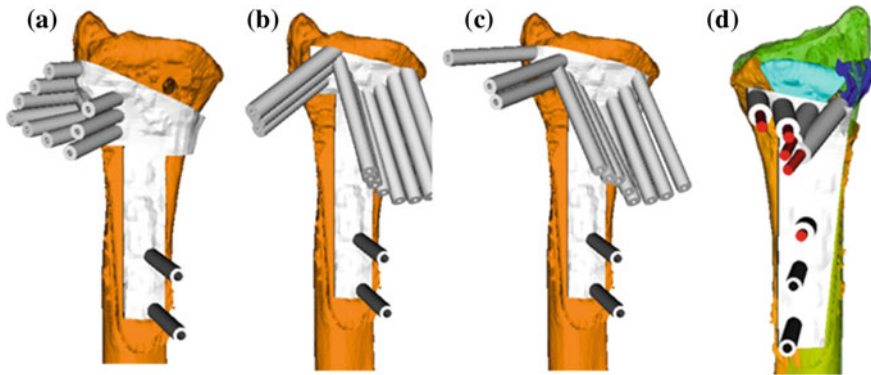


**Fig. 17** Patient-specific guides designed for a combined intra- and extra-articular distal radius osteotomy. **a–c** Three drilling guides combining six cut planes were applied to guide the intra-articular osteotomies. **d** Reduction guide for the extra-articular osteotomy

After the joint area was reconstructed, the pathological bone still showed a malposition of the shaft (Fig. 16d), requiring a correction of the radius length and epiphysis orientation with an additional extra-articular osteotomy (Fig. 16e). Once the preoperative plan was completed, patient-specific guides were designed for the intra- and extra-articular osteotomies as depicted in Fig. 17. The key idea of our outside-in approach is to mobilize complex-shaped fragments in the surgery using a drill; i.e., the curved cut is perforated by consecutive drill holes (i.e., spaced by 5 mm) using a surgical drill instead of a saw. By doing so, the exact position, direction, and depth of the drill holes can be calculated preoperatively and integrated into a guide with corresponding drill sleeves (Fig. 17a–d). The heights of the sleeves were carefully matched to the length of the drill bit to avoid entering too far into the joint. In the surgery, the holes were drilled using three drilling guides, a K-wire was inserted into the holes, and a cannulated chisel was used to connect the holes to complete the osteotomy. An additional guide was used for supporting the extra-articular osteotomy (Fig. 17d) by predrilling the screw holes of the plates as previously described.

## 5 Results and Discussion

In this chapter, we have described a technique combining 3D preoperative planning of long bone deformity correction with additive-manufactured patient-specific instruments. So far, we have applied the approach to osteotomies of the radius, ulna, humerus, femur, tibia, and fibula. The method has enabled us to perform the osteotomies more accurately and in a more controlled fashion.

Exact restoration of the normal anatomy is crucial for a satisfactory clinical outcome of orthopedic surgeries [49]. We also consider the accuracy of the procedure, i.e., how precisely the reduction is performed compared to the preoperative plan, as one of the major outcome measures. Besides demonstrating efficacy of the presented technique, accuracy evaluation provides the surgeon a quantitative control of success, enabling the minimization of technical errors and improvement of surgical skills. The accuracy of the surgical procedure can be assessed by comparing the desired planning result with the reduction performed in the surgery based on postoperative images. As in the preoperative planning, CT-based 3D evaluation is considered as the gold standard for assessing the residual deformity [11, 50]. In our case, postoperative CT images were available in several cases, acquired to assess bone consolidation during routine clinical follow-ups. Using the postoperative bone model extracted from CT, the same registration method as in the preoperative planning can be applied to quantify the difference between planned and performed reduction in 3D. We have performed CT-based accuracy evaluation of 37 surgeries, comprising different types of osteotomies and anatomy. The residual rotation error is expressed by the 3D angle of the rotation in axis-angle representation. The residual translation error is given by the length of the 3D displacement vector.

On average, the accuracy in rotation and translation for the evaluated epi-/diaphyseal osteotomies ( $n = 27$ ) was  $4.3^\circ \pm 3.6^\circ$  and  $1.9 \pm 1.3$  mm, respectively. For intra-articular osteotomies ( $n = 10$ ) an average residual angulation and displacement  $4.7^\circ \pm 3.5^\circ$  and  $0.9 \pm 0.5$  mm, respectively, was assessed with the method described in [11]. Figure 18 demonstrates the comparison between the planning and the postoperative 3D model of the 4-part intra-articular distal radius osteotomy presented in Sect. 4. In this case, a rotational error of less than  $2^\circ$  and a translational error below 2 mm were achieved. One year after surgery, the patient had symmetric strength and range of motion of her wrist and was pain free. The measured errors are slightly higher compared to in-vitro experiments [27, 51], where an average

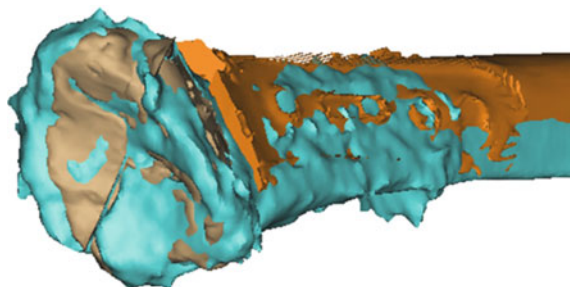


**Fig. 18** Postoperative accuracy evaluation of the combined intra- and extra-articular osteotomy presented in Sect. 4. The preoperative plan (*brown and orange fragments*) are aligned with the postoperative bone model (*cyan*) obtained from postoperative CT scans. Note that the intra-articular fragments of the preoperative plan (*brown*) were virtually fused to make the registration more robust (Color figure online)

accuracy of  $1^\circ/1$  mm was reported for distal radius osteotomies performed with a similar technique. Several other studies have evaluated the feasibility and accuracy in a clinical setting for the forearm bones [29–31], the humerus [52], and the lower extremities [34]. In these studies, an average deviation from the 3D preoperative plan between  $1^\circ$  and  $5^\circ$  was measured after surgery, but the evaluation was only performed on postoperative radiographs.

Computerized preoperative planning offers high accuracy and satisfactory results for surgical outcome; nevertheless, it still presents some challenges to be considered carefully. Preoperatively defining the reduction target (i.e., the goal model) correctly is a major contributor to a successful planning. So far, the contralateral bone has been proved to be the best reconstruction template available [12, 18] although considerable bilateral asymmetry may exist [39–41]. Even in case of perfect symmetry, soft tissues may have a considerable influence on the joint function. Consequently, a successful clinical outcome cannot always be ensured by merely relying on the contralateral bone anatomy, even if the reduction is performed precisely as planned. The integration of a pre- and postoperative motion simulation into the preoperative planning application may be the next step to better predict the functional outcome [53] for soft tissue injuries. Apart from this, the resolution of the image data used for planning and the subsequent segmentation process are additional technical factors, which may also influence the planning accuracy. Nevertheless, bone models extracted from CT scans with an axial resolution of 1 mm and using interactive segmentation methods, such as thresholding and region growing, have been shown to be sufficiently accurate for preoperative planning [54]. Intraoperatively, the correct placement of the guide(s) on the bone also has a major impact on the accuracy of the entire procedure, because the reduction is computed relative to the osteotomy site. Therefore, all means should be taken to ensure a precise identification of the intended guide position intra-operatively. One first step verification is to check the fit of the guide on real-size replica of the bone anatomy, manufactured with laser sintering devices. For a precise fit in the surgery, the bone should be debrided from periosteum as much as possible. Nevertheless, for finding a stable fit on regularly shaped surfaces such as the cylindrical mid-shaft region, manual measurements with respect to anatomical reference points may still be necessary, which is a limitation of the presented method.

We have had different experiences regarding the two different types of reduction guides described in Sect. 3. Using the technique based on pre-drilling the screw holes of the implant, we have observed some difficulties in achieving the correct reduction for osteotomies where extensive soft tissue tension was present (e.g., opening wedge distal radius or tibia osteotomies). Particularly in these cases, separate reduction guides appeared to be more suited and more accurate. An additional benefit of separate reduction guides is that dedicated parts of the guide body, such as wedges, can be used in addition to the K-wires to further improve the control of the reduction. However, guide generation is more time-consuming for multi-part reduction guides and the exposure of the bone must be larger. Due to the limited access to the bone, the separate reduction guide and additionally required K-wires may complicate surgical procedures such as sawing or implant fixation.

**Table 1** Average time necessary for generating a computer-based preoperative plan for three different categories of complexity

	Category I	Category II	Category III
Surgical plan	Simple: opening-wedge or single-cut shaft osteotomies	Medium: closing wedge osteotomies, two-bone osteotomies (radius-ulna, tibia-fibula)	Complex: intra-articular osteotomies, double osteotomies
Guide design	Simple and standardized: one pre- and one postoperative guide	Medium: three or more guides	Complex: more than three, highly individualized guides
Average planning time (h)	2.1 ± 0.8 h (n = 16)	4.0 ± 0.9 h (n = 20)	9.1 ± 3.7 h (n =28)

In the future, patient-specific osteosynthesis plates with additional functionality, such as supporting the surgeon in the reduction, may be a promising alternative to combine the advantages of the present guiding techniques. Moreover, the possibility of using patient-specific osteosynthesis implants, integrated into the preoperative plan and fitted to the patient anatomy, would also improve the evident problem of the poor fitting of anatomical standard-plates. Recently, the application of a first patient-specific implant prototype has been demonstrated in-vitro [55]. However, its high manufacturing costs over 1000 USD limit its wide-spread clinical application. Selective laser melting, which has proven to be highly productive in other medical fields, may allow for a cost-effective fabrication in the future.

Long planning times and the necessary effort have been seen as disadvantages of computer-assisted preoperative planning approaches as the one presented herein. We have evaluated the time required for our preoperative planning including the guide design based on 64 cases. The cases were assigned to one of three different categories dependent on their complexity with respect to the surgical plan and/or the patient-specific instruments. Table 1 summarizes the average planning times for each category.

Compared to the conventional approach, an additional cost of €250 (\$340 USD) per case arises due to guide manufacturing. Moreover, the radiation exposure for the patient may be higher due to the increased use of preoperative CT imaging. Nevertheless, the technique may reduce total fluoroscopy time in the surgery.

In conclusion, 3D planning has become an integral part of the preoperative assessment for long bone deformities at our institution. While simpler corrective osteotomies can be efficiently planned in a standardized way using dedicated planning tools, more complex cases still require a laborious manual effort, resulting in considerable personnel costs. Considering these cases, further research must be performed to reduce the preoperative planning time. Additive manufacturing has revolutionized computer-assisted surgery. Patient-specific surgical guides provide an efficient and accurate way of implementing a computer-based surgical plan in the surgery. As the preoperative plan and the surgical technique are closely linked,



training of the surgeons in using surgical guides is essential. After gaining practical experience, the technique may reduce operation times and enables osteotomy corrections that were not possible before, e.g., complex intra-articular osteotomies [11]. As a next future step, the extension of the method to other anatomy, such as bones of the wrist or foot, will be studied.

## References

1. Cambron J, King T (2006) The bone and joint decade: 2000 to 2010. *J Manipulative Physiol Ther* 29(2):91–92
2. Brooks PM (2006) The burden of musculoskeletal disease—a global perspective. *Clin Rheumatol* 25(6):778–781
3. Woolf AD, Pfleger B (2003) Burden of major musculoskeletal conditions. *Bull World Health Organ* 81(9):646–656
4. Wade RH, New AM, Tselentakis G, Kuiper JH, Roberts A, Richardson JB (1999) Malunion in the lower limb. A nomogram to predict the effects of osteotomy. *J Bone Joint Surg Br* 81(2):312–316
5. Honkonen SE (1995) Degenerative arthritis after tibial plateau fractures. *J Orthop Trauma* 9(4):273–277
6. Nagy L, Jankauskas L, Dumont CE (2008) Correction of forearm malunion guided by the preoperative complaint. *Clin Orthop Relat Res* 466(6):1419–1428
7. Jayakumar P, Jupiter JB (2014) Reconstruction of malunited diaphyseal fractures of the forearm. *Hand* 9(3):265–273
8. Lustig S, Khiami F, Boyer P, Catonne Y, Deschamps G, Massin P (2010) Post-traumatic knee osteoarthritis treated by osteotomy only. *Orthop Traumatol Surg Res* 96(8):856–860
9. Espinosa N (2012) Total ankle replacement. Preface. *Foot Ankle Clin* 17(4):xiii–xiv
10. Parratte S, Boyer P, Piriou P, Argenson JN, Deschamps G, Massin P (2011) Total knee replacement following intra-articular malunion. *Orthop Traumatol Surg Res* 97(6 Suppl): S118–S123
11. Schweizer A, Fürnstahl P, Nagy L (2013) Three-dimensional correction of distal radius intra-articular malunions using patient-specific drill guides. *J Hand Surg Am* 38(12):2339–2347
12. Mast J, Teitge R, Gowda M (1990) Preoperative planning for the treatment of nonunions and the correction of malunions of the long bones. *Orthop Clin North Am* 21(4):693–714
13. Paley D (2002) Principles of deformity correction. Springer, Berlin. ISBN:354041665X
14. Marti RK, Heerwaarden RJ, Arbeitsgemeinschaft für Osteosynthesefragen (2008) Osteotomies for posttraumatic deformities: Thieme Stuttgart. ISBN:3131486716
15. Fernandez DL (1982) Correction of post-traumatic wrist deformity in adults by osteotomy, bone-grafting, and internal fixation. *J Bone Joint Surg Am* 64(8):1164–1178
16. Paley D (2011) Intra-articular osteotomies of the hip, knee, and ankle. *Oper Tech Orthop* 21(2):184–196
17. Ring D, Prommersberger KJ, Gonzalez del Pino J, Capomassi M, Slullitel M, Jupiter JB (2005) Corrective osteotomy for intra-articular malunion of the distal part of the radius. *J Bone Joint Surg Am* 87(7):1503–1509
18. Schweizer A, Fürnstahl P, Harders M, Szekely G, Nagy L (2010) Complex radius shaft malunion: osteotomy with computer-assisted planning. *Hand* 5(2):171–178
19. Bilic R, Zdravkovic V, Boljevic Z (1994) Osteotomy for deformity of the radius. Computer-assisted three-dimensional modelling. *J Bone Joint Surg Br* 76(1):150–154
20. Zdravkovic V, Bilic R (1990) Computer-assisted preoperative planning (CAPP) in orthopaedic surgery. *Comput Methods Programs Biomed* 32(2):141–146

21. Langlotz F, Bachler R, Berlemann U, Nolte LP, Ganz R (1998) Computer assistance for pelvic osteotomies. *Clin Orthop Relat Res* 354:92–102
22. Jaramaz B, Hafez MA, DiGioia AM (2006) Computer-assisted orthopaedic surgery. *Proc IEEE* 94(9):1689–1695
23. Athwal GS, Ellis RE, Small CF, Pichora DR (2003) Computer-assisted distal radius osteotomy. *J Hand Surg Am* 28(6):951–958
24. Wang G, Zheng G, Gruetzner PA, Mueller-Alsbach U, von Recum J, Staubli A et al (2005) A fluoroscopy-based surgical navigation system for high tibial osteotomy. *Technol Health Care* 13(6):469–483
25. Hufner T, Kendoff D, Citak M, Geerling J, Krettek C (2006) Precision in orthopaedic computer navigation. *Orthopade* 35(10):1043–1055
26. Sarment DP, Sukovic P, Clinthorne N (2003) Accuracy of implant placement with a stereolithographic surgical guide. *Int J Oral Maxillofac Implants* 18(4):571–577
27. Ma B, Kunz M, Gammon B, Ellis RE, Pichora DR (2014) A laboratory comparison of computer navigation and individualized guides for distal radius osteotomy. *Int J Comput Assist Radiol Surg* 9(4):713–724
28. Kunz M, Ma B, Rudan JF, Ellis RE, Pichora DR (2013) Image-guided distal radius osteotomy using patient-specific instrument guides. *J Hand Surg Am.* 38(8):1618–1624
29. Miyake J, Murase T, Moritomo H, Sugamoto K, Yoshikawa H (2011) Distal radius osteotomy with volar locking plates based on computer simulation. *Clin Orthop Relat Res* 469(6):1766–1773
30. Miyake J, Murase T, Oka K, Moritomo H, Sugamoto K, Yoshikawa H (2012) Computer-assisted corrective osteotomy for malunited diaphyseal forearm fractures. *J Bone Joint Surg Am* 94(20):e150
31. Murase T, Oka K, Moritomo H, Goto A, Yoshikawa H, Sugamoto K (2008) Three-dimensional corrective osteotomy of malunited fractures of the upper extremity with use of a computer simulation system. *J Bone Joint Surg Am* 90(11):2375–2389
32. Schweizer A, Frnstahl P, Nagy L (2014) Three-dimensional planing and correction of osteotomies in the forearm and the hand. *Ther Umsch* 71(7):391–396
33. Tricot M, Duy KT, Docquier PL (2012) 3D-corrective osteotomy using surgical guides for posttraumatic distal humeral deformity. *Acta Orthop Belg* 78(4):538–542
34. Victor J, Premanathan A (2013) Virtual 3D planning and patient specific surgical guides for osteotomies around the knee: a feasibility and proof-of-concept study. *Bone Joint J* 95-B (11 Suppl A):153–158
35. Koch PP, Muller D, Pisan M, Fucentese SF (2013) Radiographic accuracy in TKA with a CT-based patient-specific cutting block technique. *Knee Surg Sports Traumatol Arthrosc* 21(10):2200–2205
36. Lorensen WE, Cline HE (1987) Marching cubes: a high resolution 3D surface construction algorithm. In: *ACM SIGGRAPH computer graphics*, ACM. ISBN:0897912276
37. Chen Y, Medioni G (1992) Object modelling by registration of multiple range images. *Image Vis Comput* 10(3):145–155
38. Mount DM, Arya S (1998) ANN: library for approximate nearest neighbour searching
39. Dumont CE, Pfirrmann CW, Ziegler D, Nagy L (2006) Assessment of radial and ulnar torsion profiles with cross-sectional magnetic resonance imaging. A study of volunteers. *J Bone Joint Surg Am* 88(7):1582–1588
40. Matsumura N, Ogawa K, Kobayashi S, Oki S, Watanabe A, Ikegami H et al (2014) Morphologic features of humeral head and glenoid version in the normal glenohumeral joint. *J Shoulder Elbow Surg* 23(11):1724–1730
41. Vroemen JC, Dobbe JG, Jonges R, Strackee SD, Streekstra GJ (2012) Three-dimensional assessment of bilateral symmetry of the radius and ulna for planning corrective surgeries. *J Hand Surg Am* 37(5):982–988
42. Horn BK (1987) Closed-form solution of absolute orientation using unit quaternions. *JOSA A* 4(4):629–642

43. Meyer DC, Siebenrock KA, Schiele B, Gerber C (2005) A new methodology for the planning of single-cut corrective osteotomies of mal-aligned long bones. *Clin Biomech* (Bristol, Avon) 20(2):223–227
44. Miniaci A, Ballmer F, Ballmer P, Jakob R (1989) Proximal tibial osteotomy: a new fixation device. *Clin Orthop Relat Res* 246:250–259
45. Fujisawa Y, Masuhara K, Shiomi S (1979) The effect of high tibial osteotomy on osteoarthritis of the knee. An arthroscopic study of 54 knee joints. *Orthop Clin North Am* 10(3):585–608
46. Schneider P, Eberly DH (2002) *Geometric tools for computer graphics*. Morgan Kaufmann, Burlington ISBN:0080478026
47. Moreland J, Bassett L, Hankaer G (1987) Radiographic analysis of the axial alignment of the lower extremity. *J Bone Joint Surg Am* 69(5):745–749
48. Fabri A, Pion S (2009) CGAL: the computational geometry algorithms library. In: *Proceedings of the 17th ACM SIGSPATIAL international conference on advances in geographic information systems*, ACM. ISBN:1605586498
49. Schemitsch EH, Richards RR (1992) The effect of malunion on functional outcome after plate fixation of fractures of both bones of the forearm in adults. *J Bone Joint Surg Am* 74(7):1068–1078
50. Kendoff D, Lo D, Goleski P, Warkentine B, O’Loughlin PF, Pearle AD (2008) Open wedge tibial osteotomies influence on axial rotation and tibial slope. *Knee Surg Sports Traumatol Arthrosc* 16(10):904–910
51. Oka K, Murase T, Moritomo H, Goto A, Nakao R, Sugamoto K et al (2011) Accuracy of corrective osteotomy using a custom-designed device based on a novel computer simulation system. *J Orthop Sci* 16(1):85–92
52. Takeyasu Y, Oka K, Miyake J, Kataoka T, Moritomo H, Murase T (2013) Preoperative, computer simulation-based, three-dimensional corrective osteotomy for cubitus varus deformity with use of a custom-designed surgical device. *J Bone Joint Surg Am* 95(22):e173
53. Furnstahl P, Schweizer A, Nagy L, Szekely G, Harders M (2009) A morphological approach to the simulation of forearm motion. In: *Conference proceedings of IEEE engineering medicine biology society*, pp 7168–71
54. Oka K, Murase T, Moritomo H, Goto A, Sugamoto K, Yoshikawa H (2009) Accuracy analysis of three-dimensional bone surface models of the forearm constructed from multidetector computed tomography data. *Int J Med Robot* 5(4):452–457
55. Omori S, Murase T, Kataoka T, Kawanishi Y, Oura K, Miyake J et al (2014) Three-dimensional corrective osteotomy using a patient-specific osteotomy guide and bone plate based on a computer simulation system: accuracy analysis in a cadaver study. *Int J Med Robot* 10(2):196–202